R. & M. No. 2934
(15,292)
A.R.C. Technical Report

MINISTRY OF SUPPLY

AERONAUTICAL RESEARCH COUNCIL
REPORTS AND MEMORANDA

Measurements of Two-dimensional Derivatives on a Wing–Aileron–Tab System with a 1541 Section Aerofoil

PART I.—Direct Aileron Derivatives

By

K. C. WIGHT,
of the Aerodynamics Division, N.P.L.

LONDON: HER MAJESTY'S STATIONERY OFFICE
1955
FIVE SHILLINGS NET

Measurements of Two-dimensional Derivatives on a Wing–Aileron–Tab System with a 1541 Section Aerofoil

PART I.—Direct Aileron Derivatives

By

K. C. WIGHT,
of the Aerodynamics Division, N.P.L.

Reports and Memoranda No. 2934*
October, 1952

Summary.—Measurements have been made of the direct two-dimensional damping and stiffness derivatives for a 20 per cent aileron on an aerofoil with a 1541 section in incompressible flow.

Corrections arising from the apparatus are discussed and reference is made to an attempt to measure the direct tab derivatives.

The effects are shown of frequency parameter, amplitude of oscillation, Reynolds number, aileron angle and position of transition on the wing.

Variation with frequency parameter is substantially the same as for vortex-sheet theory and variation of amplitude produces little change in both derivatives. At the lowest Reynolds number there is little change in both derivatives with variation of aileron angle $\bar{\beta}$ for the condition of natural transition, but at higher Reynolds numbers the stiffness derivatives increase at $\bar{\beta} = -8$ deg.

A forward movement of transition reduces the stiffness derivatives at the smaller aileron angles, but at $\bar{\beta} = -8$ deg, at the lowest Reynolds number, an increase results.

Similar trends are observed for the damping derivatives above $\omega = 1$.

Comparison with vortex-sheet theory shows that the measured values of the stiffness $(-h_{\beta})$ and damping $(-h_{\dot{\beta}})$ derivatives are approximately 0·6 of the theoretical values.

1. *Introduction.*—The measurements described in this report form part of an investigation to obtain complete sets of two-dimensional wing–aileron–tab derivatives in a 9-ft × 7-ft low-speed wind tunnel. The aerofoil constructed for this purpose was one with a 1541 section, 15 per cent thickness-chord ratio and $12\frac{1}{2}$-deg trailing-edge angle. It was fitted with a 20 per cent aileron and a 4·2 per cent (approx.) tab.

The report presents results obtained for the direct aileron derivatives with the 1541 section (Fig. 1), showing the effects of the following variables : frequency parameter, Reynolds number, amplitude of oscillation, position of transition on the wing and mean aileron angle. Reference is also made to a preliminary attempt to measure the direct tab derivatives, which was abandoned due to excessive tab distortion.

* Published with the permission of the Director, National Physical Laboratory.

2. *Apparatus.*—A brief description of the apparatus and technique has already been given in Ref. 1, but for the present application the following minor changes were made. The steel-strip balance was re-designed and two similar balances constructed one for use with the aileron and the other for use with the tab. Improvement in constancy of calibration and stability of zero was effected by stabilizing the light sources[2], and greater accuracy was achieved by increased gain in the indicator. The reference voltage generators originally used were re-designed and now have permanent magnet fields. On the mechanical side, back-lash in the system was reduced and this extended the frequency range for reliable measurement from 10 c.p.s. to 13 c.p.s. At this frequency the steel strips in use give a rise in response of approximately 2 per cent for both balances. Dynamic calibration was carried out as described in Ref. 1.

3. *Details of Model.*

Section	1541*
Thickness/chord ratio	15 per cent
Trailing-edge angle	$12\frac{1}{2}$ deg
Span	72 in.
Wing chord	30 in.
Aileron chord	6 in.
Tab chord	1·25 in.
Wing-aileron gap	0·06 in.
Aileron-tab gap	0·04 in.

The model was constructed mainly of pine with two mahogany spars and a set of ribs of sandwich construction, the framework thus formed being covered with a pine skin 0·125 in. (approx.) thick. The aileron was of similar box construction, and the tab was of solid mahogany.

Both aileron and tab hinges were crossed-spring bearings, which allowed maximum amplitudes of oscillation of 5 deg and were located as shown in Fig. 2. In addition, provision was made for setting each control-surface angle without deflecting the spring bearings. Graduated quadrants formed links between aileron and tab and a spring bearing on each driving wire. A vernier on each quadrant enabled settings to be made to an accuracy of $\pm 0{\cdot}05$ deg.

The whole model was finished in black Phenoglaze, which forms a hard surface and polishes well.

4. *Arrangement of Aerofoil in Tunnel.*—The aerofoil was mounted horizontally between false walls in order to avoid effects of the tunnel boundary layer (Fig. 3). A gap of approximately 0·1 in. was left between the ends of the aerofoil and the false walls, which extended from the tunnel roof to the floor.

The wing was carried by cantilever members (A and B, Fig. 3), extending through clearance holes in the false walls and tunnel walls and fixed to rigid supports outside the tunnel. Support A was housed in a streamlined fairing. Support B was a relatively open structure and caused little blockage to the stream. The forcing station was at approximately mid-span.

5. *Calibration of Tunnel.*—It was found initially that pulsations occurred in the air stream, which at the higher wind speeds were of sufficient magnitude to produce strong vibration of the working-section. Investigation with a pressure pick-up showed that the pulsations were present to a small extent even with the tunnel empty, but the addition of the false walls and aerofoil mountings increased their strength more than eight times. The pulsation frequency ranged from 0 to 30 c.p.s. and was proportional to the speed of the tunnel fan.

* The aerofoil designed for these experiments was a 1541 section, number NPL 282. Subsequent measurements on the model showed that the trailing-edge angle was $12\frac{1}{2}$ deg and not 15 deg as appropriate to that number,

An examination of the flow in the tunnel showed that the effect was due to the false walls and cantilever model supports slowing down the flow in the neighbourhood of the tunnel walls and thus inducing a separation at the walls of the diffuser. This occurred mainly on the inside of the return circuit, and led to stalling of the tips of the fan.

The pulsation strength with the false walls in position was reduced to less than $\frac{1}{16}$ of its value by the addition of trailing-edge flaps set at an angle of 4 deg towards the tunnel walls to speed up the flow at these points, as shown in Fig. 3.

With the aerofoil absent, variation of the velocity in the tunnel section occupied by the model was found to be less than 1 per cent from the mean value except near the false walls. Measurements in the boundary layer near the false walls at the position occupied by the centre of the aerofoil section showed a drop in ρV^2 of approximately 12 per cent at 0·5 in. from the wall.

6. *Transition Positions.*—The positions of the natural transition were determined by the liquid-film technique[3] at Reynolds numbers of approximately 1, 2 and 3 million. The transition positions were approximately the same on both surfaces, at $0{\cdot}68c$ for $R = 1 \times 10^6$ moving forward to $0{\cdot}65c$ for $R = 3 \times 10^6$.

Derivative measurements were also made with the transition fixed at $0{\cdot}1c$ and $0{\cdot}4c$, on both upper and lower surfaces by means of wires attached to the surfaces and stretched spanwise across the model[4].

7. *Notation*

H		Hinge moment per unit span
	$=$	$H_\beta\beta + H_{\dot\beta}\dot\beta$
β		Angular displacement from mean position
β_0		Amplitude of oscillation
$\bar\beta$		Mean aileron angle
h_β	$=$	$H_\beta/\rho V^2c^2$
$h_{\dot\beta}$	$=$	$H_{\dot\beta}/\rho Vc^3$
ρ		Density
V		Wind speed
c		Aerofoil chord
R		Reynolds number
f		Frequency
ω		Frequency parameter
	$=$	$2\pi fc/V$

8. *Measurements.*—Initially measurements of the direct tab derivatives were made, but large errors were found to be present due to twist of the tab under the aerodynamic loading. A method of correction was devised, but this required an accurate knowledge of the distortion mode present, which was difficult to determine. In view of this and the large errors indicated, the tests were abandoned until a stiffer tab could be constructed. It was estimated that with a tab of magnesium alloy the errors due to twist would be small.

The aileron derivative measurements were made with the tab locked to the aileron, and the tab driving wire and quadrant were removed. A frequency range from 3 to 13 c.p.s. was covered for every combination of Reynolds number, aileron angle and transition position for an amplitude of 5 deg. The same frequency range was covered for $2\frac{1}{2}$ deg amplitude, but variation of the other parameters, as indicated in the following table, was less extensive.

Amplitude β_0 (deg)	Reynolds number (approx.) R	Transition position	Aileron angle $\bar{\beta}$ (deg)
5	1, 2 and 3 $\times$ 10^6	Natural, $0{\cdot}4c$ $0{\cdot}1c$	4, 0, -4, -8
$2{\cdot}5$	1×10^6	Natural	0, -4, -8
$2{\cdot}5$	1, 2 and 3 $\times$ 10^6	$0{\cdot}1c$	0
$2{\cdot}5$	1×10^6	$0{\cdot}1c$	-8

The corresponding approximate frequency parameter ranges are tabulated below for each Reynolds number.

Reynolds number R	Frequency parameter ω
1×10^6	$0{\cdot}72$ to $3{\cdot}14$
2×10^6	$0{\cdot}36$ to $1{\cdot}57$
3×10^6	$0{\cdot}22$ to $0{\cdot}99$

Values for the stiffness derivative $-h_\beta$ corresponding to zero frequency were obtained from static measurements.

9. *Corrections.*—(*a*) *Apparatus Damping.*—The apparatus damping was determined by measuring the damping reaction in still air at each frequency with the aileron disconnected from the driving wire. A small correction had to be made for hysteresis damping forces in the spring bearings of the aileron. This was obtained by taking the difference between estimated still air damping reactions at zero frequency with the aileron connected and disconnected. These values were estimated by extrapolating curves against frequency.

(*b*) *Distortion of Model.*—Curves relating uncorrected measurements of the stiffness derivatives $-h_\beta$ to the frequency parameter ω show a marked and progressive change with Reynolds number (Fig. 4). This effect is due to flexure of the wing under the oscillatory lift forces which, for the highest wind speed and aileron amplitude, amounted to $\pm$ 160 lb (approx.), and produced a movement at the centre of the aerofoil of approximately $\pm$ $0{\cdot}05$ in. Additional reactions in the driving wire resulted from this movement, mainly through inertial coupling. When calculated values of these reactions were based on measurements of the wing displacements and an estimate of the product of inertia, they were of the correct order if the displacement was assumed to be in phase with the aileron motion.

An exact determination of the magnitude of the error was not possible without a knowledge of the wing derivatives and distortion mode. However, assuming a vertical translation of the aerofoil entirely due to the lift forces on it, approximate theoretical treatment leads to the result $\delta h_\beta = kV^2\omega^2$ for the error. The constant k was determined from measurements with transition at $0{\cdot}1c$ and aileron angle 0 deg, since the scale effect appeared to be negligible at $\omega = 0$ in this case. The slopes of curves relating h_β to V^2 for constant ω give values for $k\omega^2$ which, when plotted against ω^2, give a curve of slope k.

An attempt was made to reduce the flexure of the wing by means of stay-rods connected between earth and mid-span, but it was found difficult to provide sufficient stiffness without introducing considerable aerodynamic interference.

(*c*) *Aileron Attachments.*—Forces on the driving wires, quadrant and associated fittings, due mainly to drag, produce a small moment on the aileron which is measured as part of the stiffness derivative. The effect of the wires was calculated from wire-drag measurements, whilst that of

the remainder was determined from static experiments by the addition of dummy quadrant assemblies on each side of the existing bearing. The result gave a constant correction to h_β which amounted to approximately -4 per cent.

(*d*) *Tunnel-Wall Effects.*—No corrections have been applied for tunnel-wall effects or blockage. The static blockage (static blockage + wake blockage) amounts to $\Delta V/V = 1{\cdot}3$ per cent at the highest Reynolds number.

10. *Experimental Results*.*—(*a*) *Effect of Frequency Parameter* (*Figs.* 5 *to* 10).—The stiffness derivative $-h_\beta$ varies by not more than 16 per cent, over the ω range, for a given Reynolds number, transition position and aileron angle, the curves having in general a minimum in the neighbourhood of $\omega = 1{\cdot}0$ to $1{\cdot}5$.

The damping derivative $-h_{\dot\beta}$ shows little variation above $\omega = 1{\cdot}2$. For smaller values of ω the curves show a falling off in damping which becomes less pronounced as the aileron angle is increased or the transition moved forward.

(*b*) *Reynolds Number Effects* (*Figs.* 5 *to* 10).—Scale effect on $-h_\beta$ is small for $\bar\beta = 0$ deg, and for the natural transition case shows little increase with increasing aileron deflection until $\bar\beta = -8$ deg is reached, when increases in $-h_{\dot\beta}$ of up to 13 per cent are observed at a Reynolds number of 3×10^6. Forward movement of the transition point introduces this increase at a lower Reynolds number (2×10^6) and leads to some effect at smaller values of $\bar\beta(\pm 4$ deg).

Some effect of Reynolds number on $-h_{\dot\beta}$ was also observed. It appeared to be least for the forward transition positions with $\bar\beta = -8$ deg.

(*c*) *Effect of Aileron Angle* (*Figs.* 11 *to* 12).—At the lowest Reynolds number $-h_\beta$ shows little variation with $\bar\beta$ for the natural transition case. Forward movement of the transition produces a reduction in $-h_\beta$, which amounts to approximately 20 per cent with the transition at $0{\cdot}1c$ with $\bar\beta = 0$ deg. This reduction becomes smaller as $\bar\beta$ is increased (positively and negatively), until finally it rapidly changes sign in the neighbourhood of $\bar\beta = -8$ deg to give an increase in $-h_\beta$. At the highest Reynolds number this behaviour is modified by scale effect.

A somewhat similar, but much less pronounced, trend is visible in the curves for $-h_{\dot\beta}$ above $\omega = 1{\cdot}0$. At lower values of ω forward movement of the transition increases $-h_{\dot\beta}$, the increase being greater for higher values of $\bar\beta$.

(*d*) *Effect of Amplitude.*—Change of amplitude from $\beta_0 = 5$ deg to $2{\cdot}5$ deg has little effect on $-h_{\dot\beta}$ and produces small changes of not more than 5 per cent in $-h_\beta$. Behaviour with variation of transition position, ω, $\bar\beta$ and R is the same as for $\beta_0 = 5$ deg.

11. *Comparison with Theory.*—A comparison between vortex-sheet theory[5] and the measured values of $-h_\beta$ and $-h_{\dot\beta}$ for the natural transition, with $\bar\beta = 0$ and $R = 1 \times 10^6$, is given in Fig. 13. The form of the variation with ω is substantially the same for both theory and experiment, but the measured values of $-h_\beta$ and $-h_{\dot\beta}$ are approximately $0{\cdot}6$ of the theoretical values.

A paper by Andreopoulos, Cheilek and Donovan[6] (1949), gives derivative results from oscillatory tests on a 40 per cent flap and a 10 per cent tab, using an NACA 0010 aerofoil section. Rough agreement with vortex-sheet theory was obtained for the flap, but the derivatives for the tab appeared to be $0{\cdot}7$ (approx.) of the theoretical values at $\omega = 1{\cdot}0$. A closer approximation to vortex-sheet theory would be expected in this case since the trailing-edge angle is smaller than for the 1541 section[7].

Scruton, Raymer and Dunsdon[8] (1945) measured aileron stiffness and damping derivatives for a B.A.C. Wing type 167 of aspect ratio $9{\cdot}2$. Approximate figures for the aileron characteristics were as follows :—trailing-edge angle 18 deg, aspect ratio 11, aileron chord/wing chord 20 per cent. Comparison with vortex-sheet values gave a ratio of $0{\cdot}6$ for both stiffness and damping derivatives.

* Tabulated results are given at the end of the report.

REFERENCES

No.	Author	Title, etc.
1	J. B. Bratt and K. C. Wight	The effect of sweepback on the fundamental derivative coefficients for flexural motion. R. & M. 2774. October, 1950.
2	K. C. Wight	A note on an automatic control for maintaining constant intensity of a light source. *J. Sci. Inst.*, Vol. 28, pp. 276 to 277. September, 1951.
3	W. E. Gray	A simple visual method of recording boundary-layer transition (liquid film). R.A.E. Tech. Note Aero. 1816. April, 1946.
4	L. W. Bryant and H. C. Garner	Control testing in wind tunnels. R. & M. 2881. November, 1950.
5	I. T. Minhinnick	Tables of functions for evaluation of wing and control-surface flutter derivatives for incompressible flow. R.A.E. Report Structures 86. A.R.C. 13,730. July, 1950. (Unpublished.)
6	T. C. Andreopoulos, H. A. Cheilek and A. F. Donovan.	Measurements of the aerodynamic hinge moments of an oscillating flap and tab. U.S.A.F. Rep. No. 5874. April, 1949.
7	L. W. Bryant, A. S. Halliday and A. S. Batson.	Two-dimensional control characteristics. R. & M. 2730. March, 1950.
8	C. Scruton, W. G. Raymer and D. V. Dunsdon.	Experimental determination of the Aerodynamic derivatives for flexural-aileron flutter of B.A.C. wing type 167. R. & M. 2373. May, 1945.

TABULATED RESULTS

(*a*) *Natural Transition ; $R = 0{\cdot}94 \times 10^6$; $\beta_0 = 5$ deg*

$\bar{\beta} = +4$ deg

ω	$-h_\beta \times 10^2$	ω	$-h_{\dot{\beta}} \times 10^2$
0	1·19	—	—
0·60	1·07	0·72	0·435
1·20	1·04	1·20	0·480
1·60	1·03	1·69	0·510
2·00	1·05	2·18	0·525
2·50	1·08	2·65	0·550
3·00	1·13	3·13	0·550

$\bar{\beta} = 0$ deg

ω	$-h_\beta \times 10^2$	ω	$-h_{\dot{\beta}} \times 10^2$
0	1·21	—	—
0·60	1·09	0·73	0·440
1·20	1·05	1·22	0·490
1·60	1·05	1·72	0·505
2·00	1·07	2·21	0·525
2·50	1·09	2·67	0·535
3·00	1·12	3·16	0·540

$\bar{\beta} = -4$ deg

ω	$-h_\beta \times 10^2$	ω	$-h_{\dot{\beta}} \times 10^2$
0	1·20	—	—
0·60	1·08	0·72	0·425
1·20	1·06	1·20	0·490
1·60	1·05	1·68	0·515
2·00	1·05	2·16	0·535
2·50	1·07	2·64	0·555
3·00	1·15	3·12	0·560

$\bar{\beta} = -8$ deg

ω	$-h_\beta \times 10^2$	ω	$-h_{\dot{\beta}} \times 10^2$
0	1·20	—	—
0·60	1·07	0·73	0·470
1·20	1·05	1·21	0·505
1·60	1·05	1·70	0·535
2·00	1·06	2·18	0·555
2·50	1·08	2·67	0·575
3·00	1·12	3·16	0·575

(b) Natural Transition ; $R = 1{\cdot}89 \times 10^6$; $\beta_0 = 5$ deg

$\bar{\beta} = +4$ deg

ω	$-h_\beta \times 10^2$	ω	$-h_{\dot\beta} \times 10^2$
0	1·16	—	—
0·40	1·10	0·36	0·390
0·60	1·07	0·61	0·430
0·80	1·05	0·85	0·480
1·00	1·04	1·09	0·495
1·20	1·04	1·33	0·510
1·60	1·04	1·58	0·525

$\bar{\beta} = 0$ deg

ω	$-h_\beta \times 10^2$	ω	$-h_{\dot\beta} \times 10^2$
0	1·18	—	—
0·40	1·10	0·36	0·340
0·60	1·07	0·61	0·420
0·80	1·05	0·85	0·465
1·00	1·04	1·09	0·490
1·20	1·03	1·33	0·520
1·60	1·03	1·57	0·535

$\bar{\beta} = -4$ deg

ω	$-h_\beta \times 10^2$	ω	$-h_{\dot\beta} \times 10^2$
0	1·17	—	—
0·40	1·09	0·36	0·355
0·60	1·07	0·60	0·420
0·80	1·05	0·84	0·460
1·00	1·04	1·08	0·490
1·20	1·03	1·32	0·520
1·60	1·03	1·56	0·530

$\bar{\beta} = -8$ deg

ω	$-h_\beta \times 10^2$	ω	$-h_{\dot\beta} \times 10^2$
0	1·23	—	—
0·40	1·11	0·36	0·455
0·60	1·10	0·61	0·480
0·80	1·08	0·85	0·510
1·00	1·08	1·09	0·530
1·20	1·08	1·34	0·550
1·60	1·07	1·58	0·560

(c) Natural Transition ; $R = 2{\cdot}99 \times 10^6$; $\beta_0 = 5$ deg

$\bar{\beta} = +4$ deg

ω	$-h_\beta \times 10^2$	ω	$-h_{\dot\beta} \times 10^2$
0	1·15	—	—
0·20	1·14	0·23	0·455
0·40	1·13	0·38	0·440
0·60	1·10	0·53	0·445
0·80	1·08	0·68	0·460
1·00	1·07	0·83	0·475
—	—	0·98	0·485

$\bar{\beta} = 0$ deg

ω	$-h_\beta \times 10^2$	ω	$-h_{\dot\beta} \times 10^2$
0	1·15	—	—
0·02	1·12	0·23	0·315
0·40	1·09	0·39	0·360
0·60	1·07	0·54	0·400
0·80	1·05	0·69	0·440
1·00	1·04	0·85	0·460
—	—	1·00	0·480

$\bar{\beta} = -4$ deg

ω	$-h_\beta \times 10^2$	ω	$h_{\dot\beta} \times 10^2$
0	1·14	—	—
0·20	1·10	0·23	0·385
0·40	1·08	0·38	0·390
0·60	1·06	0·53	0·420
0·80	1·05	0·68	0·445
1·00	1·04	0·83	0·470
—	—	0·98	0·480

$\bar{\beta} = -8$ deg

ω	$-h_\beta \times 10^2$	ω	$-h_{\dot\beta} \times 10^2$
0	1·35	—	—
0·20	1·29	0·23	0·410
0·40	1·24	0·38	0·430
0·60	1·19	0·53	0·475
0·80	1·15	0·68	0·495
1·00	1·13	0·84	0·495
—	—	0·99	0·505

(*d*) *Transition at* 0·4*c* ; $R = 0{\cdot}94 \times 10^6$; $\beta_0 = 5$ *deg*

$\bar{\beta} = +4$ deg

ω	$-h_\beta \times 10^2$	ω	$-h_{\dot\beta} \times 10^2$
0	1·03	—	—
0·60	0·95	0·73	0·480
1·20	0·94	1·21	0·505
1·60	0·95	1·69	0·510
2·00	0·97	2·20	0·510
2·50	1·02	2·68	0·505
3·00	1·07	3·17	0·500

$\bar{\beta} = 0$ deg

ω	$-h_\beta \times 10^2$	ω	$-h_{\dot\beta} \times 10^2$
0	1·05	—	—
0·60	0·95	0·72	0·415
1·20	0·93	1·20	0·465
1·60	0·93	1·68	0·480
2·00	0·95	2·16	0·490
2·50	1·00	2·64	0·510
3·00	1·04	3·12	0·500

$\bar{\beta} = -4$ deg

ω	$-h_\beta \times 10^2$	ω	$-h_{\dot\beta} \times 10^2$
0	1·04	—	—
0·60	0·95	0·72	0·430
1·20	0·93	1·20	0·475
1·60	0·95	1·68	0·495
2·00	0·96	2·17	0·500
2·50	1·01	2·65	0·520
3·00	1·06	3·14	0·510

$\bar{\beta} = -8$ deg

ω	$-h_\beta \times 10^2$	ω	$-h_{\dot\beta} \times 10^2$
0	1·15	—	—
0·60	1·10	0·73	0·515
1·20	1·09	1·21	0·550
1·60	1·12	1·70	0·555
2·00	1·14	2·18	0·545
2·50	1·19	2·67	0·550
3·00	1·25	3·15	0·545

(*e*) *Transition at* 0·4*c* ; $R = 1{\cdot}89 \times 10^6$; $\beta_0 = 5$ *deg*

$\bar{\beta} = +4$ deg

ω	$-h_\beta \times 10^2$	ω	$-h_{\dot\beta} \times 10^2$
0	1·02	—	—
0·40	0·97	0·36	0·435
0·60	0·95	0·61	0·475
0·80	0·94	0·85	0·505
1·00	0·94	1·10	0·510
1·20	0·95	1·34	0·530
1·60	0·98	1·58	0·530

$\bar{\beta} = 0$ deg

ω	$-h_\beta \times 10^2$	ω	$-h_{\dot\beta} \times 10^2$
0	1·00	—	—
0·40	0·93	0·36	0·360
0·60	0·91	0·60	0·420
0·80	0·90	0·85	0·460
1·00	0·90	1·09	0·470
1·20	0·90	1·32	0·500
1·60	0·91	1·56	0·500

$\bar{\beta} = -4$ deg

ω	$-h_\beta \times 10^2$	ω	$-h_{\dot\beta} \times 10^2$
0	1·03	—	—
0·40	0·97	0·36	0·370
0·60	0·95	0·60	0·440
0·80	0·93	0·84	0·480
1·00	0·93	1·08	0·500
1·20	0·93	1·32	0·520
1·60	0·95	1·57	0·525

$\bar{\beta} = -8$ deg

ω	$-h_\beta \times 10^2$	ω	$-h_{\dot\beta} \times 10^2$
0	1·27	—	—
0·40	1·23	0·36	0·470
0·60	1·23	0·61	0·510
0·80	1·22	0·85	0·530
1·00	1·22	1·09	0·535
1·20	1·22	1·33	0·550
1·60	1·26	1·57	0·550

(*f*) *Transition at* 0·4*c* ; $R = 2{\cdot}99 \times 10^6$; $\beta_0 = 5$ *deg*

$\bar{\beta} = +4$ deg

ω	$-h_\beta \times 10^2$	ω	$-h_{\dot\beta} \times 10^2$
0	1·06	—	—
0·20	1·03	0·23	0·370
0·40	1·01	0·38	0·430
0·60	0·99	0·54	0·465
0·80	0·98	0·69	0·490
1·00	0·97	0·84	0·500
—	—	0·99	0·515

$\bar{\beta} = 0$ deg

ω	$-h_\beta \times 10^2$	ω	$-h_{\dot\beta} \times 10^2$
0	1·01	—	—
0·20	0·97	0·23	0·325
0·40	0·93	0·38	0·385
0·60	0·91	0·53	0·425
0·80	0·90	0·68	0·450
1·00	0·90	0·84	0·470
—	—	0·99	0·480

$\bar{\beta} = -4$ deg

ω	$-h_\beta \times 10^2$	ω	$-h_{\dot\beta} \times 10^2$
0	1·06	—	—
0·20	1·02	0·23	0·350
0·40	0·99	0·37	0·410
0·60	0·96	0·53	0·445
0·80	0·95	0·67	0·475
1·00	0·95	0·82	0·495
—	—	0·97	0·510

$\bar{\beta} = -8$ deg

ω	$-h_\beta \times 10^2$	ω	$-h_{\dot\beta} \times 10^2$
0	1·26	—	—
0·20	1·26	0·23	0·495
0·40	1·25	0·38	0·490
0·60	1·24	0·53	0·505
0·80	1·23	0·68	0·515
1·00	1·24	0·83	0·525
—	—	0·99	0·535

(*g*) *Transition at* 0·1*c* ; $R = 0{\cdot}94 \times 10^6$; $\beta_0 = 5$ *deg*

$\bar{\beta} = +4$ deg

ω	$-h_\beta \times 10^2$	ω	$-h_{\dot\beta} \times 10^2$
0	0·99	—	—
0·60	0·88	0·73	0·450
1·20	0·89	1·21	0·475
1·60	0·90	1·70	0·490
2·00	0·92	2·18	0·490
2·50	0·97	2·67	0·500
3·00	1·06	3·15	0·500

$\bar{\beta} = 0$ deg

ω	$-h_\beta \times 10^2$	ω	$-h_{\dot\beta} \times 10^2$
0	0·93	—	—
0·60	0·84	0·73	0·405
1·20	0·82	1·21	0·440
1·60	0·84	1·69	0·465
2·00	0·86	2·18	0·465
2·50	0·91	2·66	0·480
3·00	0·97	3·17	0·480

$\bar{\beta} = -4$ deg

ω	$-h_\beta \times 10^2$	ω	$-h_{\dot\beta} \times 10^2$
0	0·96	—	—
0·60	0·89	0·72	0·440
1·20	0·88	1·21	0·470
1·60	0·89	1·69	0·480
2·00	0·91	2·17	0·490
2·50	0·96	2·66	0·505
3·00	1·02	3·14	0·500

$\bar{\beta} = -8$ deg

ω	$-h_\beta \times 10^2$	ω	$-h_{\dot\beta} \times 10^2$
0	1·16	—	—
0·60	1·12	0·72	0·525
1·20	1·12	1·21	0·535
1·60	1·15	1·69	0·530
2·00	1·19	2·17	0·525
2·50	1·25	2·66	0·530
3·00	1·32	3·14	0·525

(h) *Transition at* 0·1*c* ; $R = 1{\cdot}89 \times 10^6$; $\beta_0 = 5$ *deg*

$\bar{\beta} = +4$ deg

ω	$-h_\beta \times 10^2$	ω	$-h_{\dot\beta} \times 10^2$
0	1·02	—	—
0·40	0·93	0·37	0·435
0·60	0·92	0·61	0·470
0·80	0·92	0·85	0·495
1·00	0·91	1·10	0·510
1·20	0·92	1·34	0·520
1·60	0·95	1·58	0·520

$\bar{\beta} = 0$ deg

ω	$-h_\beta \times 10^2$	ω	$-h_{\dot\beta} \times 10^2$
0	0·92	—	—
0·40	0·85	0·36	0·375
0·60	0·83	0·61	0·420
0·80	0·82	0·85	0·450
1·00	0·81	1·10	0·465
1·20	0·82	1·34	0·490
1·60	0·84	1·59	0·495

$\bar{\beta} = -4$ deg

ω	$-h_\beta \times 10^2$	ω	$-h_{\dot\beta} \times 10^2$
0	0·98	—	—
0·40	0·91	0·36	0·410
0·60	0·89	0·60	0·455
0·80	0·88	0·84	0·480
1·00	0·87	1·09	0·495
1·20	0·89	1·33	0·515
1·60	0·91	1·57	0·520

$\bar{\beta} = -8$ deg

ω	$-h_\beta \times 10^2$	ω	$-h_{\dot\beta} \times 10^2$
0	1·22	—	—
0·40	1·21	0·36	0·515
0·60	1·22	0·60	0·535
0·80	1·23	0·84	0·545
1·00	1·24	1·08	0·545
1·20	1·24	1·33	0·545
1·60	1·29	1·57	0·545

(i) *Transition at* 0·1*c* ; $R = 2{\cdot}99 \times 10^6$; $\beta_0 = 5$ *deg*

$\bar{\beta} = +4$ deg

ω	$-h_\beta \times 10^2$	ω	$-h_{\dot\beta} \times 10^2$
0	1·05	—	—
0·20	1·02	0·23	0·395
0·40	1·00	0·38	0·435
0·60	0·99	0·54	0·460
0·80	0·98	0·69	0·495
1·00	0·98	0·85	0·510
—	—	1·00	0·525

$\bar{\beta} = 0$ deg

ω	$-h_\beta \times 10^2$	ω	$-h_{\dot\beta} \times 10^2$
0	0·93	—	—
0·20	0·89	0·23	0·355
0·40	0·86	0·38	0·400
0·60	0·84	0·54	0·430
0·80	0·83	0·69	0·450
1·00	0·82	0·84	0·470
—	—	1·00	0·480

$\bar{\beta} = -4$ deg

ω	$-h_\beta \times 10^2$	ω	$-h_{\dot\beta} \times 10^2$
0	1·00	—	—
0·20	0·96	0·23	0·400
0·40	0·93	0·38	0·440
0·60	0·92	0·53	0·470
0·80	0·91	0·69	0·490
1·00	0·91	0·83	0·500
—	—	0·99	0·510

$\bar{\beta} = -8$ deg

ω	$-h_\beta \times 10^2$	ω	$-h_{\dot\beta} \times 10^2$
0	1·24	—	—
0·20	1·23	0·23	0·520
0·40	1·22	0·38	0·525
0·60	1·22	0·53	0·530
0·80	1·24	0·68	0·540
1·00	1·26	0·84	0·545
—	—	0·98	0·550

(*j*) *Natural transition ;* $R = 0{\cdot}94 \times 10^6$ *;* $\beta_0 = 2\frac{1}{2}$ *deg*

$\bar{\beta} = 0$ deg

ω	$-h_\beta \times 10^2$	ω	$-h_{\dot{\beta}} \times 10^2$
0	1·11	—	—
0·60	1·07	0·72	0·470
1·20	1·07	1·43	0·530
1·60	1·08	2·15	0·535
2·00	1·10	3·11	0·545
2·50	1·13	—	—
3·00	1·18	—	—

$\bar{\beta} = -4$ deg

ω	$-h_\beta \times 10^2$	ω	$-h_{\dot{\beta}} \times 10^2$
0	1·24	—	—
0·60	1·05	0·72	0·425
1·20	1·05	1·43	0·515
1·60	1·06	2·15	0·550
2·00	1·08	3·10	0·555
2·50	1·11	—	—
3·00	1·16	—	—

$\bar{\beta} = -8$ deg

ω	$-h_\beta \times 10^2$	ω	$-h_{\dot{\beta}} \times 10^2$
0	1·21	—	—
0·60	1·09	0·72	0·470
1·20	1·08	1·43	0·560
1·60	1·08	2·15	0·570
2·00	1·09	3·11	0·545
2·50	1·10	—	—
3·00	1·12	—	—

(*k*) *Transition at* 0·1*c ;* $R = 0{\cdot}94 \times 10^6$ *;* $\beta_0 = 2\frac{1}{2}$ *deg*

$\bar{\beta} = 0$ deg

ω	$-h_\beta \times 10^2$	ω	$-h_{\dot{\beta}} \times 10^2$
0	0·86	—	—
0·60	0·83	0·72	0·435
1·20	0·84	1·43	0·470
1·60	0·86	2·15	0·470
2·00	0·89	3·10	0·460
2·50	0·94	—	—
3·00	1·00	—	—

$\bar{\beta} = -8$ deg

ω	$-h_\beta \times 10^2$	ω	$-h_{\dot{\beta}} \times 10^2$
0	1·17	—	—
0·60	1·09	0·71	0·560
1·20	1·13	1·43	0·575
1·60	1·16	2·14	0·550
2·00	1·20	3·09	0·505
2·50	1·26	—	—
3·00	1·30	—	—

(*l*) *Transition at* 0·1*c ;* $R = 1{\cdot}89 \times 10^6$ *;* $\beta_0 = 2\frac{1}{2}$ *deg*

$\bar{\beta} = 0$ deg

ω	$-h_\beta \times 10^2$	ω	$-h_{\dot{\beta}} \times 10^2$
0	0·82	—	—
0·40	0·81	0·36	0·380
0·60	0·80	0·72	0·450
0·80	0·80	1·07	0·475
1·00	0·81	1·56	0·485
1·20	0·82	—	—
1·60	0·85	—	—

(*m*) *Transition at* 0·1*c ;* $R = 2{\cdot}99 \times 10^6$ *;* $\beta_0 = 2\frac{1}{2}$ *deg*

$\bar{\beta} = 0$ deg

ω	$-h_\beta \times 10^2$	ω	$-h_{\dot{\beta}} \times 10^2$
0	0·83	—	—
0·20	0·82	0·23	0·440
0·40	0·82	0·45	0·455
0·60	0·82	0·68	0·475
0·80	0·83	0·98	0·491
1·00	0·84	—	—

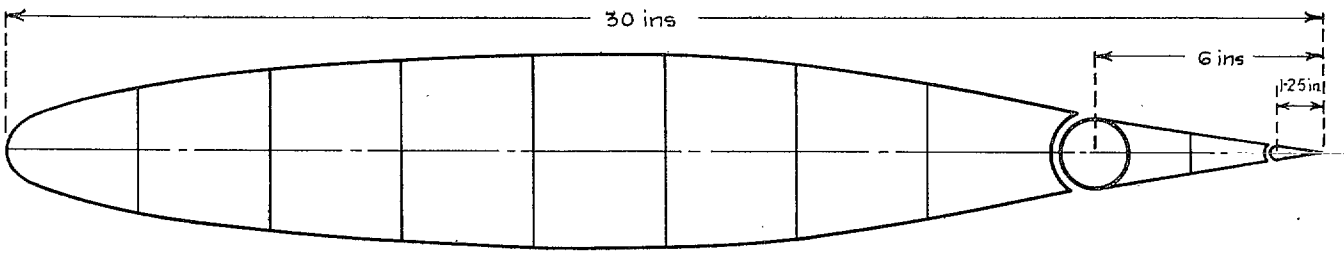

FIG. 1. Profile of aerofoil.

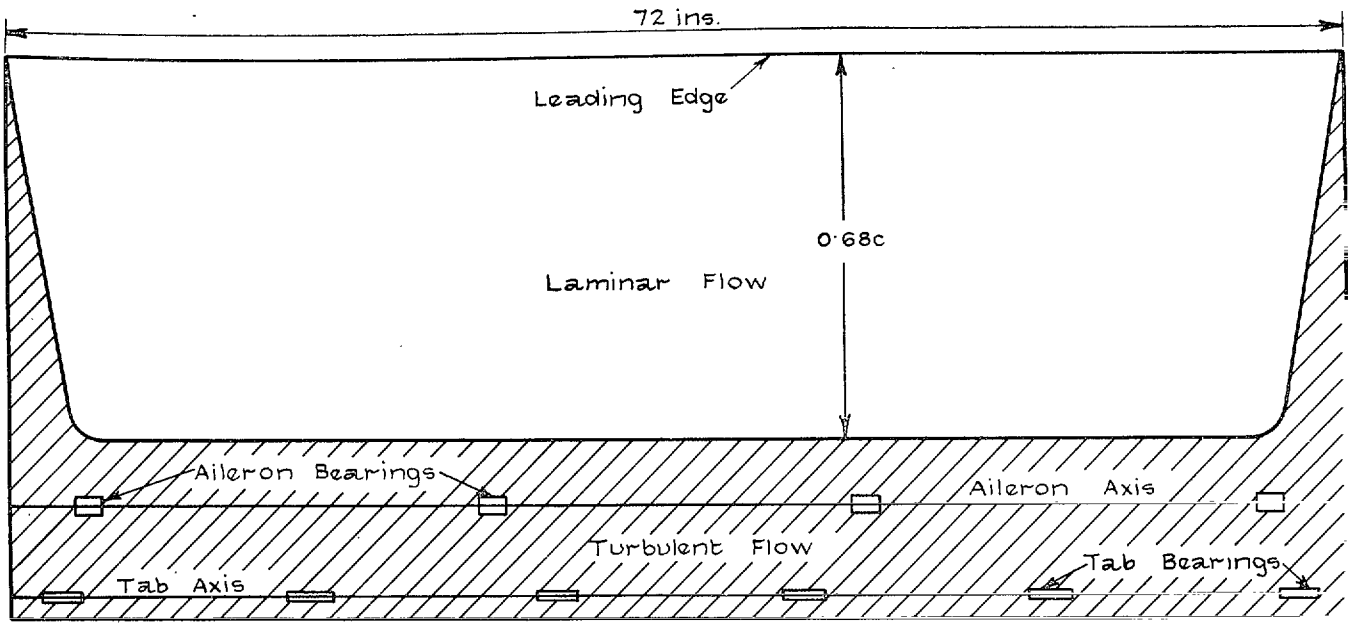

FIG. 2. Plan of aerofoil showing natural transition at $R = 0{\cdot}94 \times 10^6$.

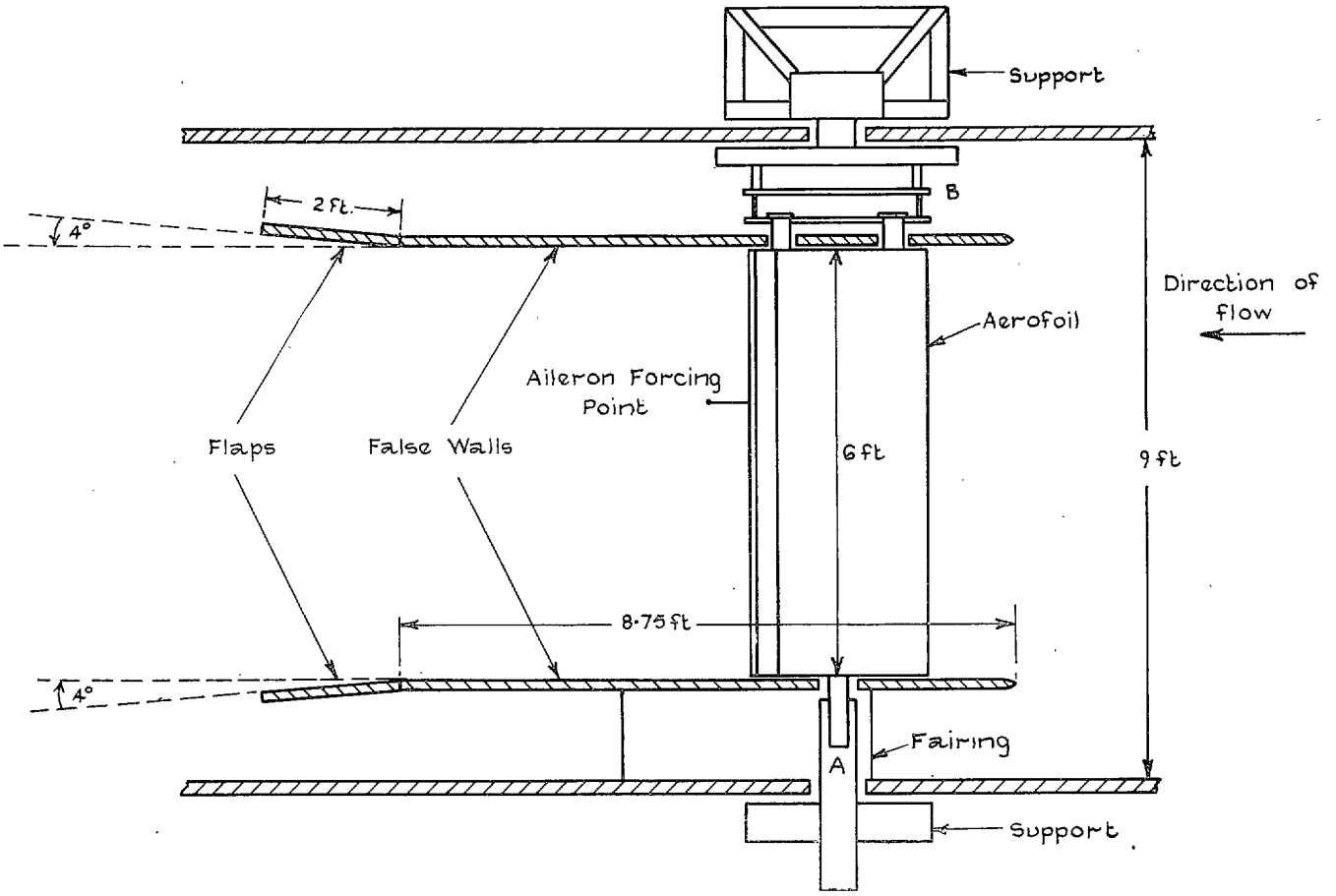

FIG. 3. Plan view of aerofoil mounting and false walls in the tunnel.

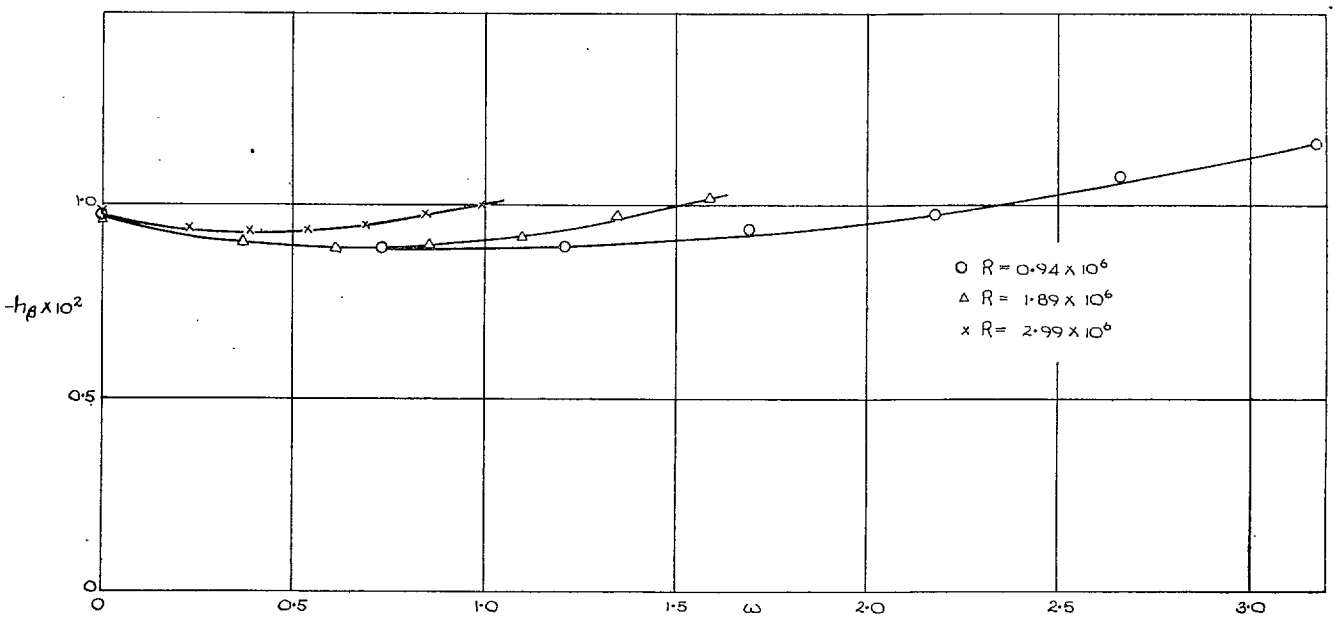

FIG. 4. Effect of wing flexure on h_β for $\bar{\beta} = 0$ deg and transition at $0{\cdot}1c$.

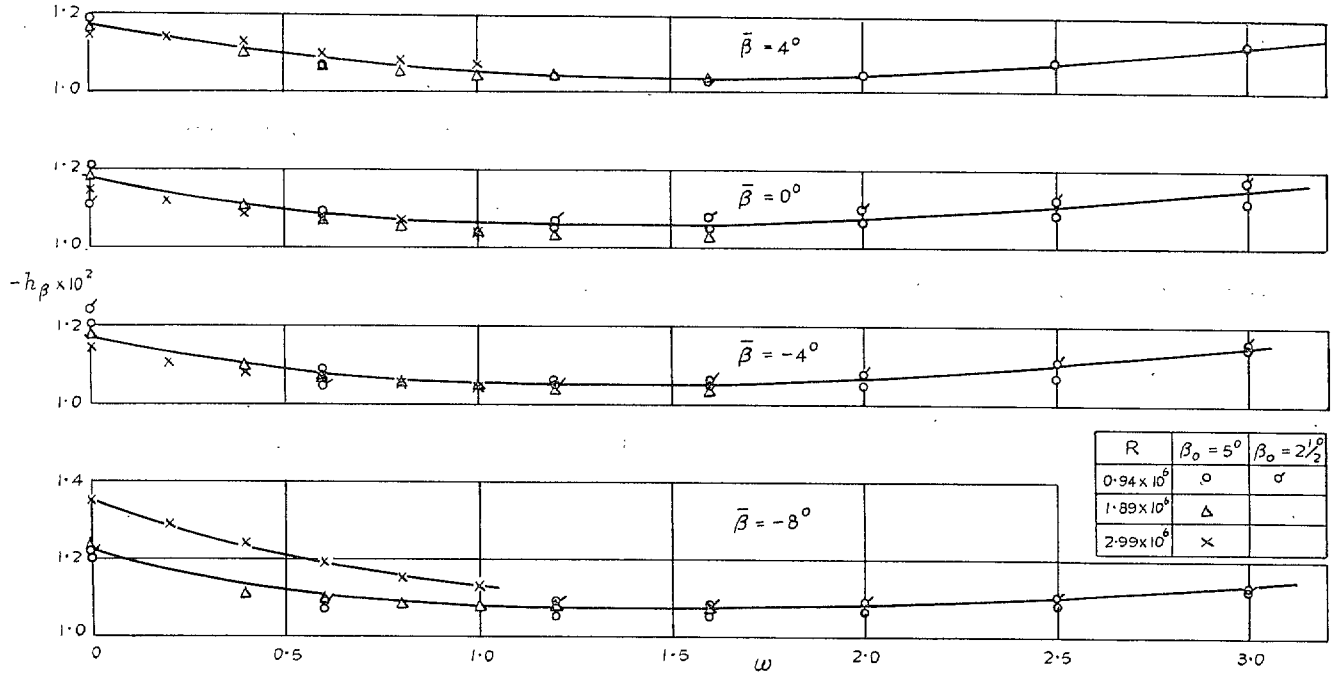

FIG. 5. Variation of h_β with frequency parameter. Natural transition.

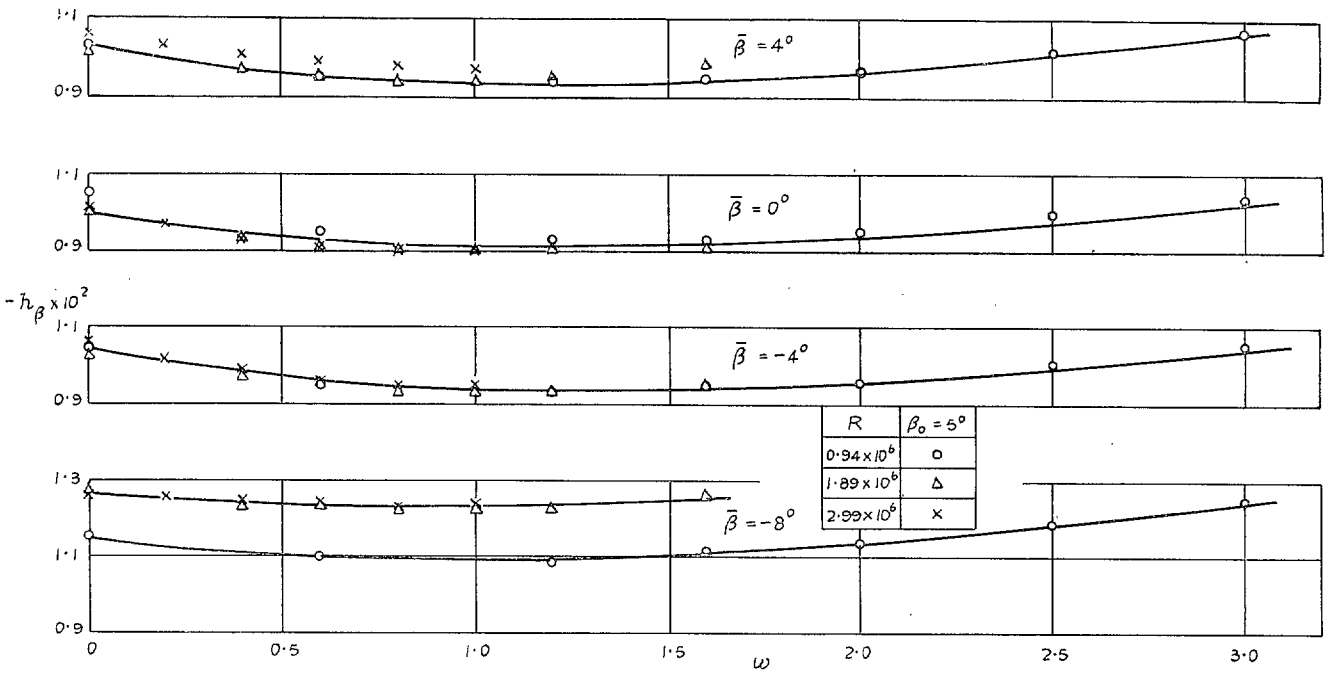

FIG. 6. Variation of h_β with frequency parameter. Transition at $0{\cdot}4c$.

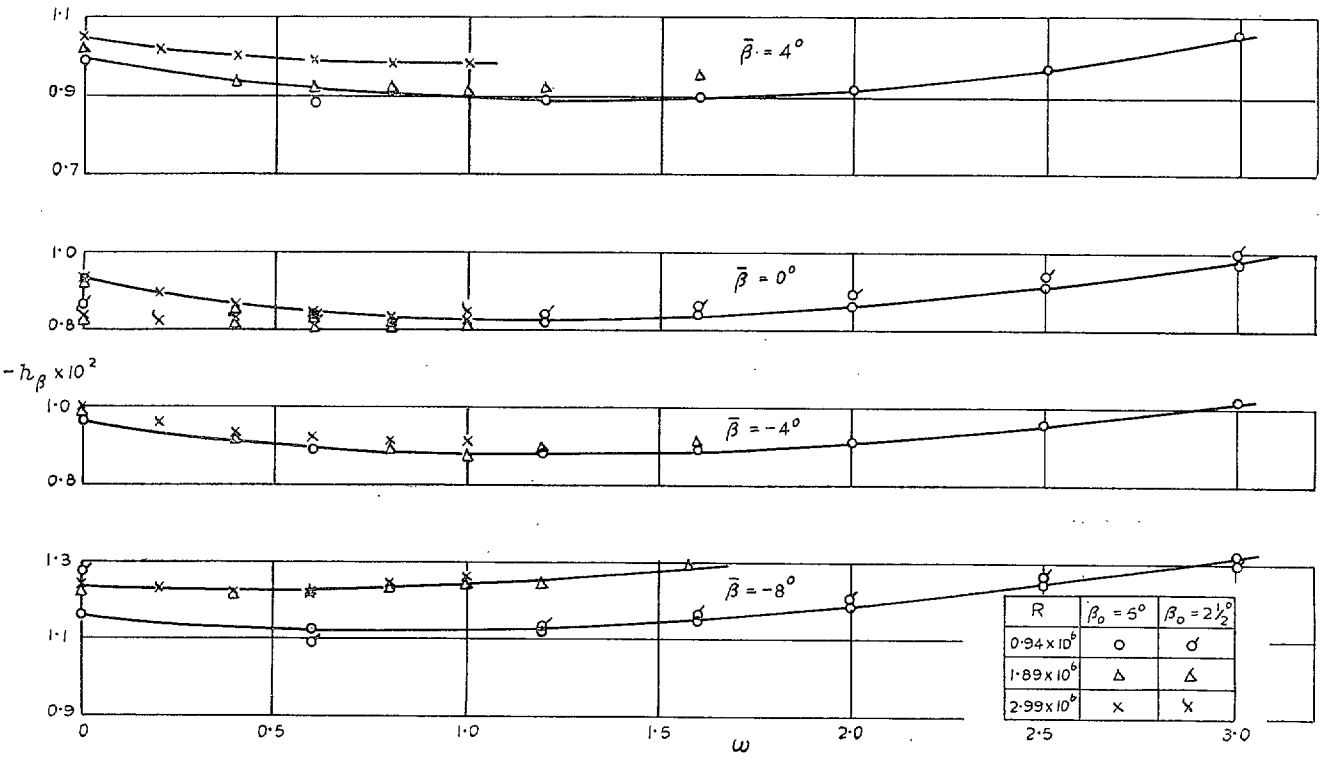

FIG. 7. Variation of h_β with frequency parameter. Transition at $0{\cdot}1c$.

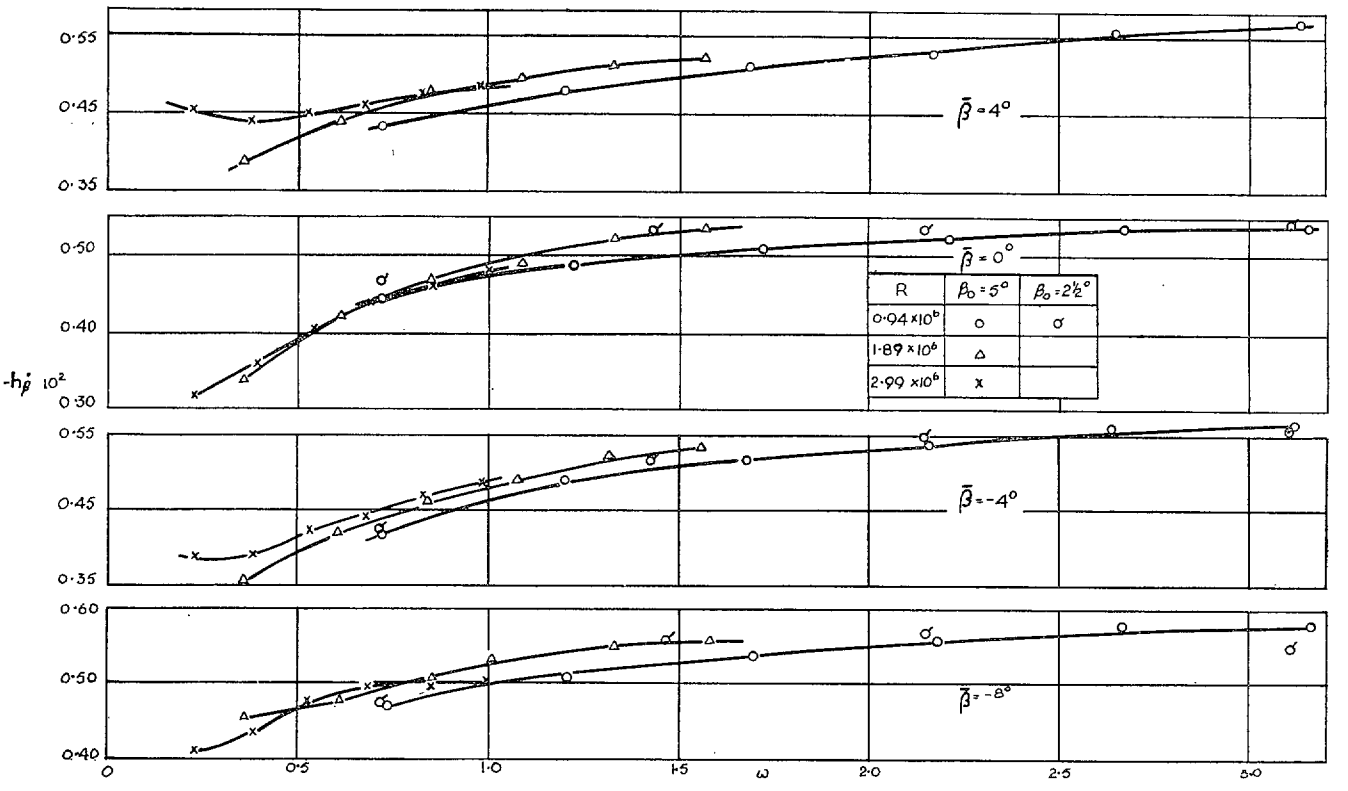

FIG. 8. Variation of $h_{\dot{\beta}}$ with frequency parameter. Natural transition.

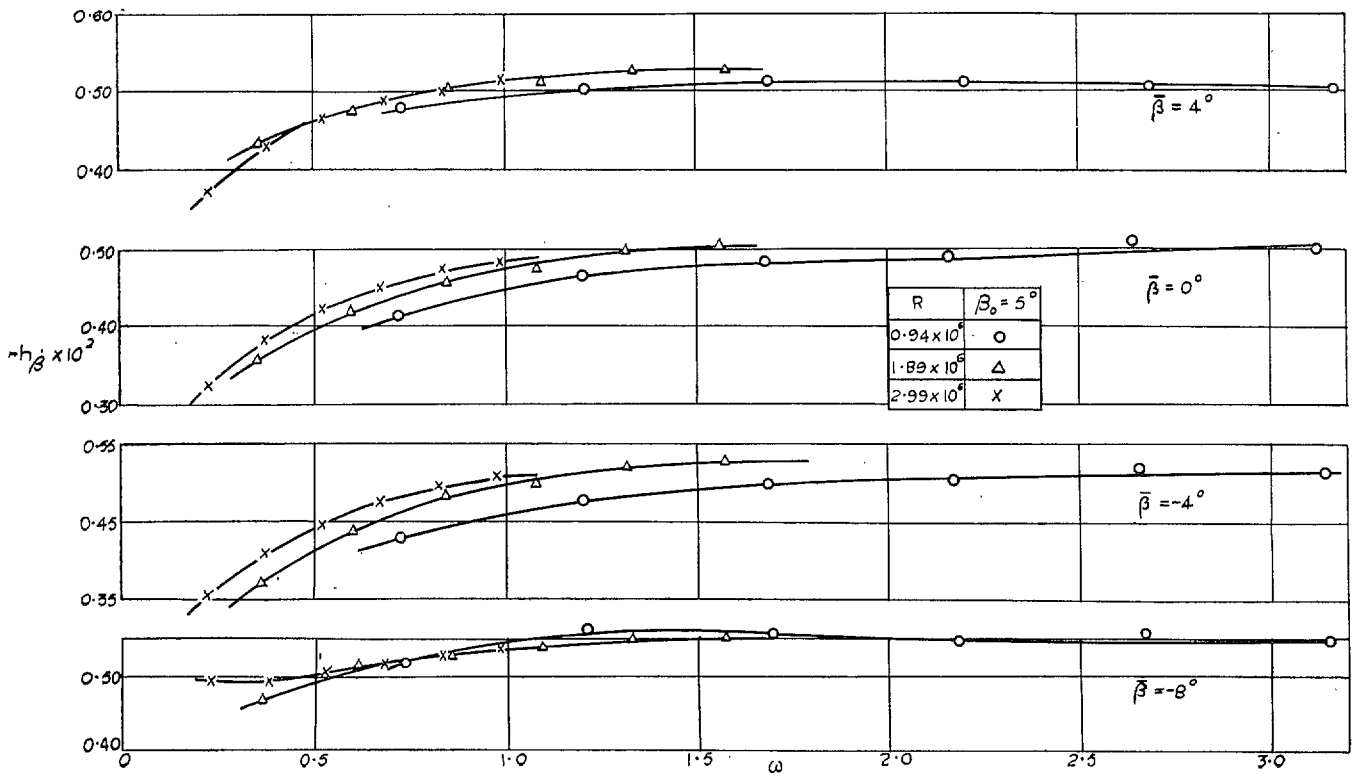

FIG. 9. Variation of $h_{\dot{\beta}}$ with frequency parameter. Transition at $0{\cdot}4c$.

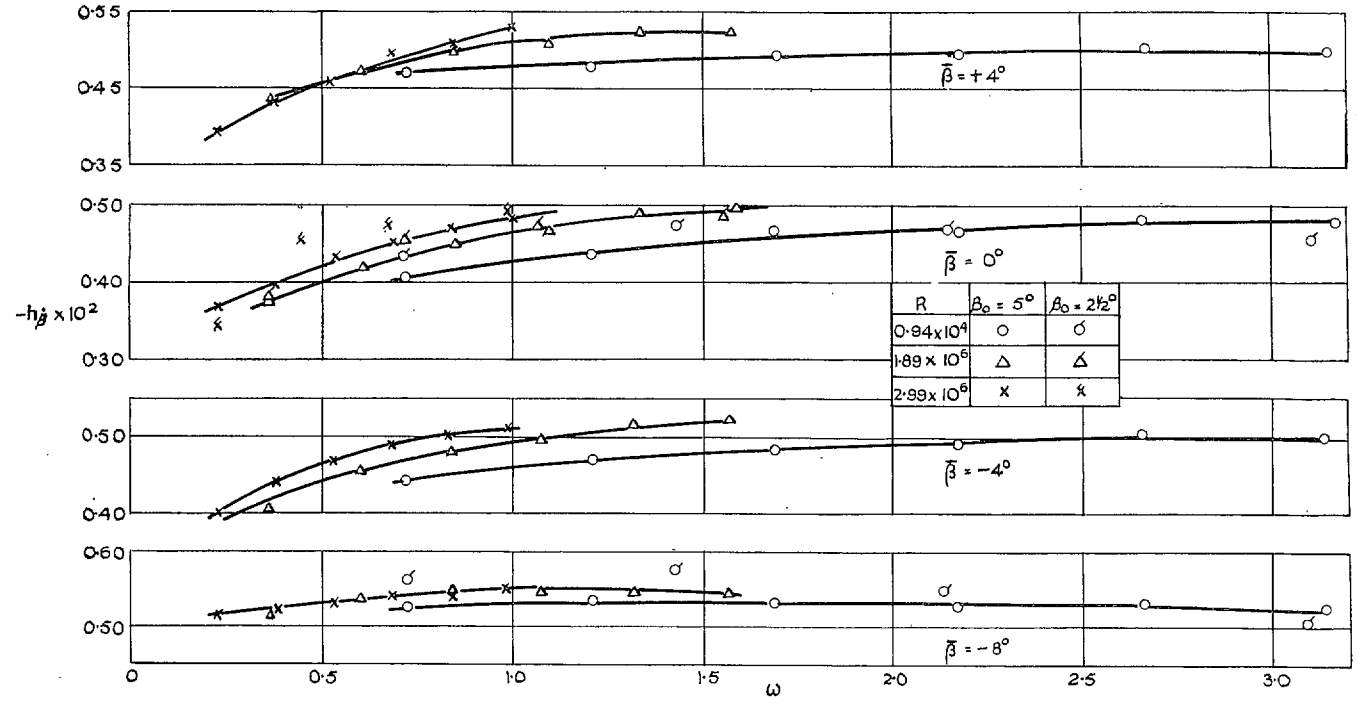

FIG. 10. Variation of $h_{\dot{\beta}}$ with frequency parameter. Transition at $0{\cdot}1c$.

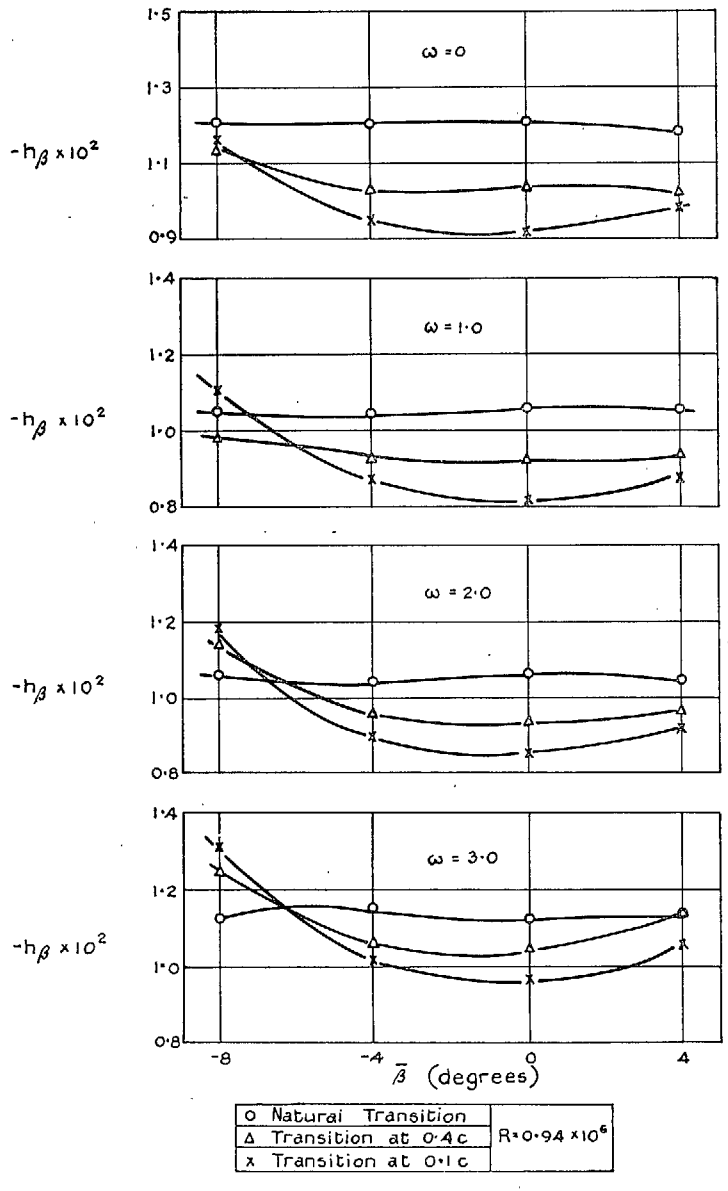

FIG. 11. Variation of h_β with aileron angle.

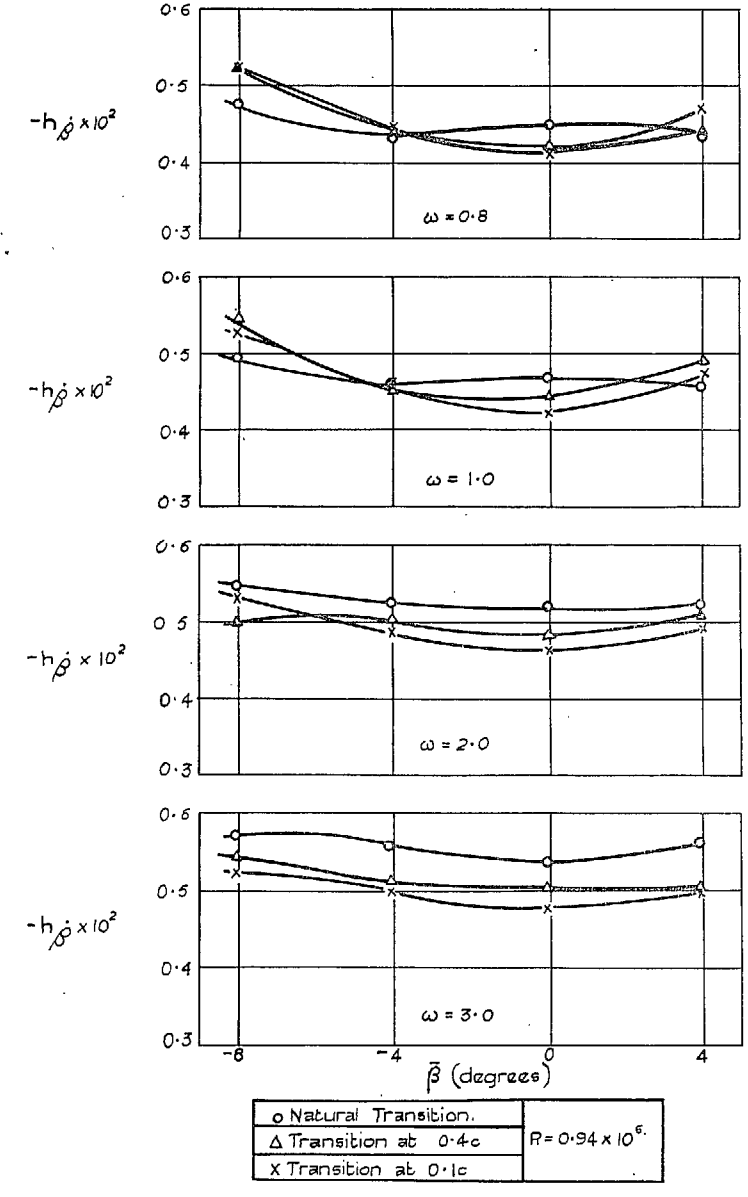

FIG. 12. Variation of $h_{\dot\beta}$ with aileron angle.

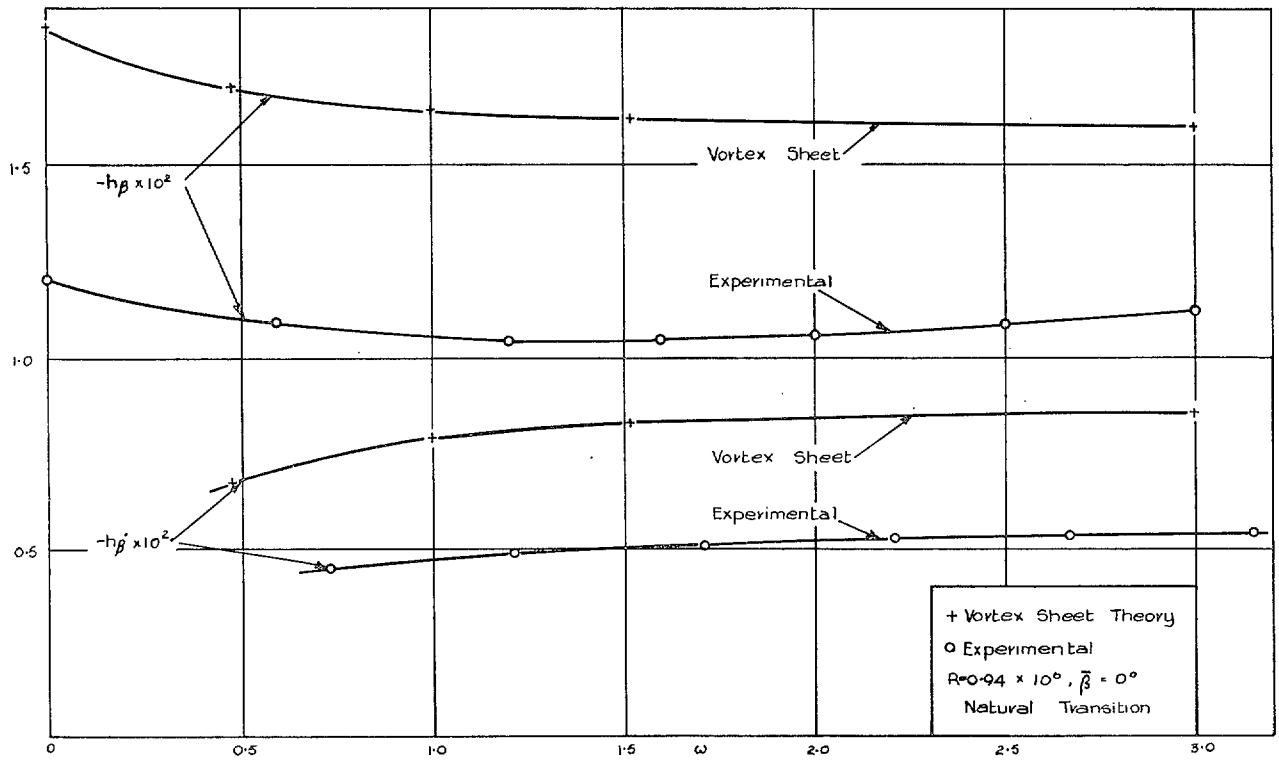

FIG. 13. Comparison with vortex-sheet theory.

J4329 Wt.18/9296 K7 7/55 D&Co. 34/263

PRINTED IN GREAT BRITAIN

Publications of the Aeronautical Research Council

ANNUAL TECHNICAL REPORTS OF THE AERONAUTICAL RESEARCH COUNCIL (BOUND VOLUMES)

1936 Vol. I. Aerodynamics General, Performance, Airscrews, Flutter and Spinning. 40*s*. (41*s*. 1*d*).

Vol. II. Stability and Control, Structures, Seaplanes, Engines, etc. 50*s*. (51*s*. 1*d*.)

1937 Vol. I. Aerodynamics General, Performance, Airscrews, Flutter and Spinning. 40*s*. (41*s*. 1*d*.)

Vol. II. Stability and Control, Structures, Seaplanes, Engines, etc. 60*s*. (61*s*. 1*d*.)

1938 Vol. I. Aerodynamics General, Performance, Airscrews. 50*s*. (51*s*. 1*d*.)

Vol. II. Stability and Control, Flutter, Structures, Seaplanes, Wind Tunnels, Materials. 30*s*. (31*s*. 1*d*.)

1939 Vol. I. Aerodynamics General, Performance, Airscrews, Engines. 50*s*. (51*s*. 1*d*.)

Vol. II. Stability and Control, Flutter and Vibration, Instruments, Structures, Seaplanes, etc. 63*s*. (64*s*. 2*d*.)

1940 Aero and Hydrodynamics, Aerofoils, Airscrews, Engines, Flutter, Icing, Stability and Control, Structures, and a miscellaneous section. 50*s*. (51*s*. 1*d*.)

1941 Aero and Hydrodynamics, Aerofoils, Airscrews, Engines, Flutter, Stability and Control, Structures. 63*s*. (64*s*. 2*d*.)

1942 Vol. I. Aero and Hydrodynamics, Aerofoils, Airscrews, Engines. 75*s*. (76*s*. 3*d*.)

Vol. II. Noise, Parachutes, Stability and Control, Structures, Vibration, Wind Tunnels. 47*s*. 6*d*. (48*s*. 7*d*.)

1943 Vol. I. Aerodynamics, Aerofoils, Airscrews, 80*s*. (81*s*. 4*d*.)

Vol. II. Engines, Flutter, Materials, Parachutes, Performance, Stability and Control, Structures. 90*s*. (91*s*. 6*d*.)

1944 Vol. I. Aero and Hydrodynamics, Aerofoils, Aircraft, Airscrews, Controls. 84*s*. (85*s*. 8*d*.)

Vol. II. Flutter and Vibration, Materials, Miscellaneous, Navigation, Parachutes, Performance, Plates, and Panels, Stability, Structures, Test Equipment, Wind Tunnels. 84*s*. (85*s*. 8*d*.)

ANNUAL REPORTS OF THE AERONAUTICAL RESEARCH COUNCIL—

1933–34	1*s*. 6*d*. (1*s*. 8*d*.)	1937	2*s*. (2*s*. 2*d*.)
1934–35	1*s*. 6*d*. (1*s*. 8*d*.)	1938	1*s*. 6*d*. (1*s*. 8*d*.)
April 1, 1935 to Dec. 31, 1936.	4*s*. (4*s*. 4*d*.)	1939–48	3*s*. (3*s*. 2*d*.)

INDEX TO ALL REPORTS AND MEMORANDA PUBLISHED IN THE ANNUAL TECHNICAL REPORTS, AND SEPARATELY—

April, 1950 – – – – R. & M. No. 2600. 2*s*. 6*d*. (2*s*. 7½*d*.)

AUTHOR INDEX TO ALL REPORTS AND MEMORANDA OF THE AERONAUTICAL RESEARCH COUNCIL—

1909–1949 – – – – – R. & M. No. 2570. 15*s*. (15*s*. 3*d*.)

INDEXES TO THE TECHNICAL REPORTS OF THE AERONAUTICAL RESEARCH COUNCIL—

December 1, 1936 — June 30, 1939.	R. & M. No. 1850.	1*s*. 3*d*. (1*s*. 4½*d*.)
July 1, 1939 — June 30, 1945.	R. & M. No. 1950.	1*s*. (1*s*. 1½*d*.)
July 1, 1945 — June 30, 1946.	R. & M. No. 2050.	1*s*. (1*s*. 1½*d*.)
July 1, 1946 — December 31, 1946.	R. & M. No. 2150.	1*s*. 3*d*. (1*s*. 4½*d*.)
January 1, 1947 — June 30, 1947.	R. & M. No. 2250.	1*s*. 3*d*. (1*s*. 4½*d*.)
July, 1951 – – – –	R. & M. No. 2350.	1*s*. 9*d*. (1*s*. 10½*d*.)

Prices in brackets include postage.

Obtainable from

HER MAJESTY'S STATIONERY OFFICE

York House, Kingsway, London W.C.2 ; 423 Oxford Street, London W.1 (Post Orders : P.O. Box No. 569, London S.E.1) ; 13A Castle Street, Edinburgh 2 ; 39 King Street, Manchester 2 ; 2 Edmund Street, Birmingham 3 ; 109 St. Mary Street, Cardiff ; Tower Lane, Bristol 1 ; 80 Chichester Street, Belfast OR THROUGH ANY BOOKSELLER

S.O. Code No. 23-2934